



Article

Toward New AQP4 Inhibitors: ORI-TRN-002

Michael Thormann¹ , Nadine Traube¹, Nasser Yehia¹, Roland Koestler¹, Gergana Galabova¹,
Nanna MacAulay² and Trine L. Toft-Bertelsen^{2,*}

¹ Origenis GmbH, Am Klopferspitz 19A, 82152 Martinsried, Germany; roland.koestler@gmx.de (R.K.)

² Department of Neuroscience, University of Copenhagen, Blegdamsvej 3, 2200 Copenhagen, Denmark

* Correspondence: trineto@sund.ku.dk

Abstract: Cerebral edema is a life-threatening condition that can cause permanent brain damage or death if left untreated. Existing therapies aim at mitigating the associated elevated intracranial pressure, yet they primarily alleviate pressure rather than prevent edema formation. Prophylactic anti-edema therapy necessitates novel drugs targeting edema formation. Aquaporin 4 (AQP4), an abundantly expressed water pore in mammalian glia and ependymal cells, has been proposed to be involved in cerebral edema formation. A series of novel compounds have been tested for their potential inhibitory effects on AQP4. However, selectivity, toxicity, functional inhibition, sustained therapeutic concentration, and delivery into the central nervous system are major challenges. Employing extensive density-functional theory (DFT) calculations, we identified a previously unreported thermodynamically stable tautomer of the recently identified AQP4-specific inhibitor TGN-020 (2-(nicotinamide)-1,3,4-thiadiazol). This novel form, featuring a distinct hydrogen-bonding pattern, served as a template for a COSMOsim-3D-based virtual screen of proprietary compounds from Origenis™. The screening identified ORI-TRN-002, an electronic homologue of TGN-020, demonstrating high solubility and low protein binding. Evaluating ORI-TRN-002 on AQP4-expressing *Xenopus laevis* oocytes using a high-resolution volume recording system revealed an IC_{50} of $2.9 \pm 0.6 \mu\text{M}$, establishing it as a novel AQP4 inhibitor. ORI-TRN-002 exhibits superior solubility and overcomes free fraction limitations compared to other reported AQP4 inhibitors, suggesting its potential as a promising anti-edema therapy for treating cerebral edema in the future.



Citation: Thormann, M.; Traube, N.; Yehia, N.; Koestler, R.; Galabova, G.; MacAulay, N.; Toft-Bertelsen, T.L.

Toward New AQP4 Inhibitors: ORI-TRN-002. *Int. J. Mol. Sci.* **2024**, *25*, 924. <https://doi.org/10.3390/ijms25020924>

Academic Editors: Graça Soveral and Inês Vieira Da Silva

Received: 23 November 2023

Revised: 4 January 2024

Accepted: 9 January 2024

Published: 11 January 2024



Copyright: © 2024 by the authors. Licensee MDPI, Basel, Switzerland. This article is an open access article distributed under the terms and conditions of the Creative Commons Attribution (CC BY) license (<https://creativecommons.org/licenses/by/4.0/>).

Keywords: aquaporin; brain edema; water permeability

1. Introduction

Cerebral edema is the excess accumulation of fluid in the intracellular or extracellular spaces of the brain [1] and is prevalent in various acute brain injuries, where it significantly increases mortality and independently elevates the risk of adverse outcomes. Existing therapies aim at mitigating critical consequences, such as elevated intracranial pressure, yet they primarily alleviate pressure rather than prevent edema formation, often through interventions like decompressive craniectomy, in which a bone flap from the skull is removed to allow the brain to expand. Water can cross cell membranes via water channels (aquaporins (AQP)) and cotransport proteins [2]. Of the large family of AQPs expressed in the majority of cell types in the mammalian body, aquaporin 4 (AQP4) is the predominant water channel in the mammalian brain [3] and is mainly expressed in the perivascular glial endfeet at the brain–blood interface [4] and in the pia, in addition to the ependymal lining bordering the fluid-filled cavities of the brain, i.e., the cerebral ventricles [5]. This distribution has led to the suggestion that AQP4 controls water fluxes into and out of the brain parenchyma and that AQP4 plays a major role in brain edema [5–8]. With the lack of a specific inhibitor of AQP4, these studies were all based on AQP4 knock-out mice (AQP4^{−/−}), which have been found to present with several molecular changes occurring secondarily to the knock-out strategy [9–13]. To address the exact and still not fully defined role of AQP4 in brain physiology and pathophysiology, and to circumvent the side effects of AQP4 knock out, an

AQP4-specific inhibitor is a desired additional tool. The identification of molecules that inhibit specific AQP isoforms is not a simple proposition for drug discovery on account of the high level of structural conservation within the family [13]. Several chemical structures have been identified [14,15] and suggested to have AQP4-inhibitory effects. AER-270 (N-[3,5-bis (trifluoromethyl)phenyl]-5-chloro-2-hydroxybenzamide), an investigational drug that has successfully completed a Phase I study, was found to reduce central nervous system (CNS) edema [16,17]. AER-271/SIM0307 (2-([3,5-Bis(trifluoromethyl) phenyl]carbamoyl)-4-chlorophenyl dihydrogen phosphate), a soluble phosphate ester prodrug of AER-270, was found to reduce swelling in two models of CNS injury complicated by cerebral edema: water intoxication and ischemic stroke modeled by middle cerebral artery occlusion (MCAO). Of note, only 20% maximal inhibition of human AQP4 was reported by AER-270 [16]. Another drug, 2-(nicotinamide)-1,3,4-thiadiazole (TGN-020), was found to be the most potent AQP4 inhibitor based on *in silico* [14] and *in vitro* [18] methods. TGN-020 represents a peculiar compound of elusive origin that was likely first described as an AQP4 inhibitor in the application to a Japanese patent in 2006, JP2006154063. The corresponding granted patents in the US (US7659312B2) and Japan (JP4273235B2) do, however, not claim TGN-020 anymore. Here, we performed deep structural investigation of TGN-020 to elucidate the uniqueness of this compound, and to potentially generate a new starting point for the ligand-based screening and design of novel AQP4 inhibitors. Using a platform that combines artificial intelligence (AI) technologies for disease and target selection, drug design, novelty assessment, complex decision making, and evolutionary learning [16,19]. We here present a soluble and low protein-binding electronic homologue of TGN-020, the ORI-TRN-002 compound, which exerts inhibitory effects on AQP4-mediated water permeability as determined with heterologously expressed AQP4 in *Xenopus laevis* oocytes [18].

2. Results

2.1. Identification of an Electronic Homologue of TGN-020

To perform an unbiased deep structural investigation of TGN-020, we used fluid thermodynamics and quantum chemical calculations (DFT/COSMO-RS) of the previously identified AQP4-selective inhibitor TGN-020 [18] (Figure 1A). To identify the lowest energy tautomer, we subjected all potentially existing tautomeric forms (Figure 1B(i–iii)) of TGN-020 to 3D structure generation, conformational analysis, and density functional theory (DFT) energy optimization using Turbomole BP-TZVP-COSMO. The COSMO-RS phase is unlike the gas phase in that it presents an environment of high electron density. The most stable structure of TGN-020 in our unbiased approach represents a novel tautomer of the compound (Figure 1B(iii)). This one differs from the described X-ray, IR, and NMR structure [20], where TGN-020 makes strong interactions with itself (X-ray and IR) in the aprotic solvent DMSO (NMR). Notably, the carbonyl group of the amide points to the sulfur side of the thiadiazole in this compound, which is in agreement with our predictions for TGN-020. Compared to the X-ray structure of TGN-020 [20], the hydrogen-bonding pattern in the new tautomer is different in the amide and thiadiazole parts (Figure 1C,D). The new pattern was used as a template to screen for electronic bioisosteres, i.e., molecules with similar sterics and electron distribution by using COSMOSim-3D, which is able to identify such bioisosteres with high confidence [15,16] by aligning and comparing their COSMO-RS σ -surfaces. These result from quantum chemical calculations of molecules in a simulated conductor, and their histograms, the so-called σ -profiles, are widely proven to provide a very suitable and almost complete basis for the description of molecular interactions in condensed systems. COSMOSim-3D uses local σ -profiles on a spatial grid and measures intermolecular similarities based on the 3D representation of the surface polarization charge densities σ of the target and the probe molecule. The probe molecule is translated and rotated in space to maximize the sum of local σ -profile similarities between the target and probe. This sum, the COSMOSim3D similarity, is a powerful descriptor of ligand similarity and allows for good discrimination between bioisosters and random pairs. With density functional theory (DFT) geometry optimization, which is performed by moving the

atoms of the molecule to obtain the most stable structure with the lowest possible ground state energy, we obtain both the lowest energy forms and their COSMO-RS σ -surfaces. The new TGN-020 tautomer was used as the target template (Figure 1E) to screen the Origenis proprietary compound library and the corresponding optimized conformers and their COSMO surfaces using a COSMOsim-3D search [16]. We identified ORI-TRN-002 (Figure 1F) as the most similar compound in our collection based on the COSMOsim-3D search (Figure 1G). This compound recapitulates the peculiar hydrogen-bonding pattern of the new form of TGN-020 almost perfectly in shape and electronic distribution, although their chemical structures vary strongly due to distinct hydrogen-bonding patterns.

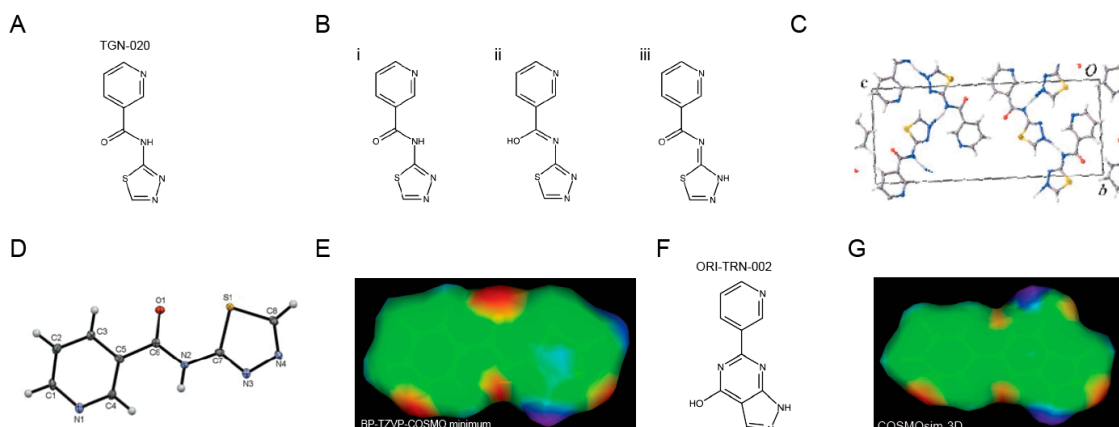
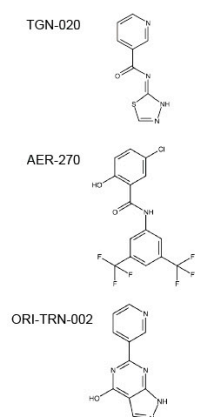


Figure 1. Identification of an electronic homologue of TGN-020. Commonly used chemical structure of TGN-020 (A). Three tautomers of TGN-020 (B). Unit cell of TGN-020 X-ray structure (C). TGN-020 X-ray structure (D). COSMO-RS surface of the most stable conformer of TGN-020 (B(iii)), displaying shape and hydrogen-bonding pattern (red, HB acceptor; blue, HB donor) (E). Chemical structure of ORI-TRN-002 (F). COSMO-RS surface of ORI-TRN-002, displaying shape and hydrogen-bonding pattern (red, HB acceptor; blue, HB donor), aligned with (E,G).

2.2. ORI-TRN-002 Displays Drug-like Properties

To evaluate the potential drug-like properties of the electronic homologue ORI-TRN-002, we measured the compound's properties in the Origenis BRAINstorm™ platform. This platform uses affinity chromatography under standard conditions and standard calibrants to measure compound properties with high accuracy and reproducibility. It allows us to assess important physicochemical properties of the compound, i.e., human and rat serum albumin affinities ($\log K_{aHSA}$ and $\log K_{aRSA}$); the percentage of binding to human plasma proteins (hPPB%); alpha acid glycoprotein affinity ($\log K_{aAGP}$); unbound fraction in liver and hepatocytes ($f_{u,liver}$ and $f_{u,hep}$); and the octanol–water distribution coefficient at pH = 7.4 ($\log D$), which is an appropriate descriptor of lipophilicity and indicator of solubility (Figure 2); and others, to finally derive tissue-specific free fractions and tissue distribution early in the process ensuring the best possible optimization of compounds for their planned application. ORI-TRN-002 (Figure 2) displays drug-like physicochemical properties similar those of to TGN-020, such as aqueous solubility, which is critical to drug delivery, and hydrophobicity, both of which play key roles in drug absorption, transport, and distribution (Figure 2). It supersedes the solubility and free fraction limitations of the Aeromics/Simcere drug AER-270 [21] (Figure 2). ORI-TRN-002 requires no prodrug approach and serves as an ideal starting point for further optimization.



ID	logD	logKaHSA	hPPB%	logKaRSA	logKaAGP	fu, liver	fu, hep
TGN-020	0.04	3.51	68.20	2.72	1.18	1.00	0.92
AER-270	3.31	5.46	99.50	5.26	6.94	<0.01	<0.01
ORI-TRN-002	-0.07	2.99	39.20	2.89	1.88	1.00	0.95

Figure 2. ORI-TRN-002 displays drug-like properties. The chemical structures of the three AQP4 inhibitors studied and their measured physico-chemical properties (logD at pH 7.4, log₁₀ of molar human serum albumin affinity constant, percent human plasma protein binding, log₁₀ of human alpha acid glycoprotein affinity constant, unbound fraction in liver, and unbound fraction in hepatocytes).

2.3. ORI-TRN-002-Mediated Inhibition of AQP4

To resolve ORI-TRN-002's inhibitory effect on AQP4, rat AQP4 (rAQP) was heterologously expressed in *Xenopus laevis* oocytes, and the AQP4-mediated water permeability was quantified. Following the introduction of an abrupt hyposmotic challenge (−100 mOsm), we determined the osmotic water permeability of the oocytes during the continuous recording of the oocyte volume with a high-resolution volume recording system. This experimental setup allows for the osmotic gradient to be introduced at a faster rate than the rate of cell volume change and sufficiently fast data acquisition to obtain several data points at the initial linear part of the cell volume change, which is required to obtain the osmotic water permeability of an AQP-expressing oocyte. The native oocyte membrane has a low inherent water permeability, thus the uninjected oocytes display a negligible background (see Figure 3A for summarized data on osmotic water permeabilities; compare $0.21 \pm 0.13 \times 10^{-3} \text{ cm s}^{-1}$, $n = 9$, for uninjected oocytes to $3.80 \pm 0.33 \times 10^{-3} \text{ cm s}^{-1}$, $n = 11$, for AQP4-expressing oocytes; representative volume traces shown as insets). The oocytes were exposed to the novel drugs (or control solution) for 60 min. prior to the determination of water permeability. The established AQP4 blockers, TGN-020 and AER-270, served as positive controls. The application of ORI-TRN-002 (20 μM , 60 min, 19 °C) reduced the water permeability of AQP4-expressing oocytes (compare $3.43 \pm 0.22 \times 10^{-3} \text{ cm s}^{-1}$, $n = 11$, for non-treated AQP4-expressing oocytes to $1.39 \pm 0.13 \times 10^{-3} \text{ cm s}^{-1}$, $n = 12$, for AQP4-expressing oocytes incubated with ORI-TRN-002; $1.05 \pm 0.15 \times 10^{-3} \text{ cm s}^{-1}$, $n = 12$, for AQP4-expressing oocytes incubated with AER-270; and $0.82 \pm 0.09 \times 10^{-3} \text{ cm s}^{-1}$, $n = 12$, for AQP4-expressing oocytes incubated with TGN-020; representative volume traces shown as insets; Figure 3B). The reduced osmotic water permeability induced by ORI-TRN-002 was not caused by a toxic effect on the cells, as verified by measuring the membrane potential of the treated oocytes ($-26.2 \pm 0.62 \text{ mV}$, $n = 11$ for non-treated oocytes; $-24.4 \pm 0.74 \text{ mV}$, $n = 12$ with ORI-TRN-002 application; Figure 3C). ORI-TRN-002 thus acts as a novel blocker of AQP4-dependent water permeability.

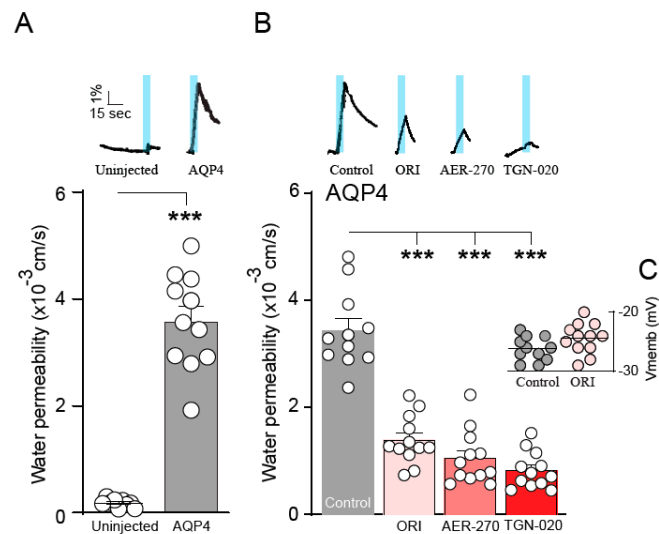


Figure 3. ORI-TRN-002-mediated inhibition of AQP4. Volume traces from an AQP4-expressing oocyte and an uninjected oocyte challenged with a hyposmotic gradient (indicated by a blue bar) (A inset). Summarized water permeabilities from uninjected—or AQP4-expressing—oocytes ($n = 11$) (A). Volume traces from an untreated AQP4-expressing oocyte or AQP4-expressing oocytes treated with ORI-TRN-002 (ORI), AER-270, or TGN-020 and challenged with a hyposmotic gradient (indicated by a blue bar) (B inset). Summarized water permeabilities from oocytes expressing AQP4, either untreated or pretreated with ORI-TRN-002 (ORI), AER-270, or TGN-020 for 60 min ($n = 11$) (B). Membrane potential monitored from the AQP4-expressing oocytes in control solution or after 60 min of pretreatment with ORI-TRN-002 (ORI) (C) ANOVA followed by Tukey's multiple comparison tests or Student's *t*-test were used as statistical test. *** $p < 0.001$.

2.4. ORI-TRN-002 Exerts an Acute Blocking Effect on AQP4

With the observation that ORI-TRN-002 inhibits AQP4 after 60 min of exposure, we subsequently measured the blocking efficacy within a shorter time frame. A time-control experiment verified the identical magnitude of water permeabilities in the AQP4-expressing oocytes as sequentially recorded at times $t = 0$ and $t = 10$ min (see summarized data in Figure 4A; compare $3.20 \pm 0.36 \times 10^{-3}$ cm s $^{-1}$, $n = 9$, for first osmotic challenge to $3.11 \pm 0.24 \times 10^{-3}$ cm s $^{-1}$, $n = 9$, for second osmotic challenge in AQP4-expressing oocytes serving as time controls; representative volume traces shown as insets). Thus, each oocyte can be used as its own control to determine the time-dependency of an inhibitor effect. Upon the acute and continuous application of 20 μ M ORI-TRN-002, we observed a decreased AQP4-mediated water permeability at $t = 10$ min (compare $3.62 \pm 0.24 \times 10^{-3}$ cm s $^{-1}$, $n = 9$, for first osmotic challenge to $1.02 \pm 0.17 \times 10^{-3}$ cm s $^{-1}$, $n = 9$, for water permeability after ORI-TRN-002 application; Figure 4A) comparable to the inhibitory effect induced by AER-270 and TGN-020 ($0.80 \pm 0.11 \times 10^{-3}$ cm s $^{-1}$, $n = 9$, after AER-270 treatment; $0.80 \pm 0.08 \times 10^{-3}$ cm s $^{-1}$, $n = 9$, with TGN-020 application; Figure 4A) without notable toxic effects (compare -25.6 ± 0.50 mV, $n = 9$, for non-treated oocytes to -26.9 ± 0.61 mV, $n = 9$, after ORI-TRN-002 application; Figure 4B). We determined the IC_{50} for ORI-TRN-002 for rAQP4 with the inclusion of different ORI-TRN-002 concentrations (IC_{50} of 2.9 ± 0.6 μ M, $n = 6$; Figure 4C). ORI-TRN-002 therefore appears to be a novel blocker of AQP4 with an acute effect.

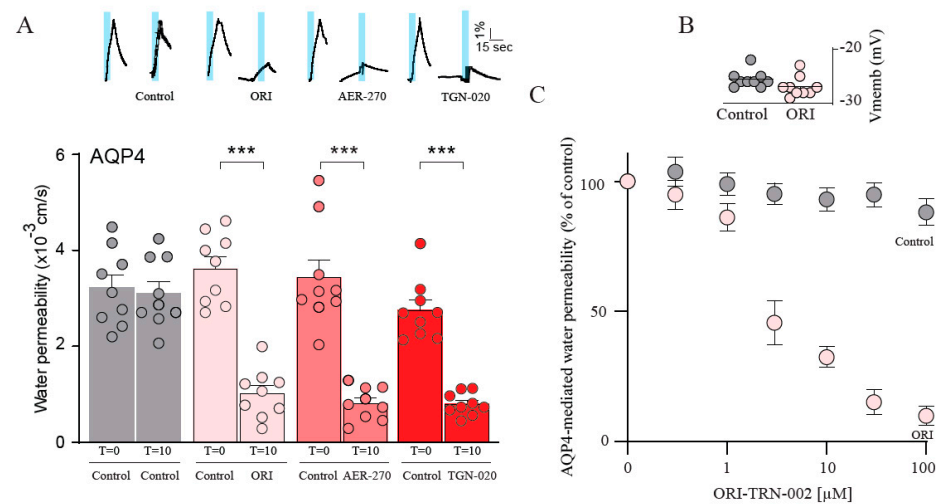


Figure 4. ORI-TRN-002 exerts an acute blocking effect on AQP4. A representative time-control experiment from an AQP4-expressing oocyte and volume traces from AQP4-expressing oocytes treated with ORI-TRN-002 (ORI), AER-270, or TGN-020 repeatedly challenged with a hyposmotic gradient (indicated by a blue bar, $t = 0$ min (control), $t = 10$ min) (A inset). Summarized water permeabilities at $t = 0$ min (control) and $t = 10$ min from oocytes expressing AQP4, either untreated or treated with ORI-TRN-002 (ORI), AER-270, or TGN-020 ($n = 9$) (A). Membrane potential monitored from the AQP4-expressing oocytes in control solution or upon treatment with ORI-TRN-002 (ORI) (B). AQP4-expressing oocytes exposed to different concentrations of ORI-TRN-002 (or vehicle (DMSO) only; ‘Control’). Data were fitted with Graphpad Prism using nonlinear regression analysis to obtain the IC_{50} from the mean of the independent regression analyses ($n = 6$) (C). ANOVA followed by Tukey’s multiple comparison tests were used as statistical test. *** $p < 0.001$.

3. Discussion

The current study reveals a novel AQP4 inhibitor, ORI-TRN-002, that significantly reduces AQP4-mediated water permeability. Due to the polarized expression in the paravascular endfeet [4] and mediated bi-directional water flux according to the imposed osmotic gradient [22], AQP4 is suggested to be implicated in a range of physiological processes [5,23]. These findings were determined using AQP4 knock-out mice with secondary changes to basic physiological parameters [9–11]. Therefore, specific blockers of AQP4 are needed as supplementary tools for the knock-out strategy in order to determine a possible role for AQP4 in humans both in physiology and in cerebral edema, where the expression of AQP4 increases [6,24], and edema size and formation is reduced when knocking-out [7] or inhibiting AQP4 [25–27]. Current therapeutic approaches focus on alleviating the critical consequences of edema, such as elevated intracranial pressure, primarily addressing pressure reduction rather than preventing edema formation. The proposed role of AQP4 in neuropathologies has heightened the importance of identifying non-toxic AQP4 activity modulators to be used for therapeutic applications. AQP drug discovery has made little progress. The small diameter of all AQP pores, together with the chemical properties of the pore-lining amino acid sidechains, means that finding drug-like compounds that can enter and block the AQPs is a challenging prospect. During the last decade, a few compounds were brought forward as potential inhibitors of AQP4, e.g., tetraethylammonium (TEA), acetazolamide, antiepileptic drugs, and bumetanide (and its derivative AqB013) [17,28–30], but all of these pharmacological agents were later demonstrated to not be effective blockers of AQP4-mediated water permeability [18,31]. Ethoxzolamide was reported to inhibit AQP4.M23 in oocytes [15]; however, this compound is a carbonic anhydrase inhibitor, and in patients, this compound may thus induce off-target effects. Other reported small molecules, despite having an appropriate affinity for AQP4 [14,15,23,32–34], have yet not passed the initial phases that allow these to be enrolled in larger clinical trials. One compound that showed an appropriate affinity for AQP4 and was reported as a novel inhibitor

by the Nakada Laboratory is TGN-020 [14,25]. The successful delivery and effect of TGN-020 to the central nervous system in vivo has been demonstrated [25], and the compound has been included in various in vitro and in vivo experimental designs [14,18,25,33], with a full screening on all AQP isoforms validating the isoform-specificity of TGN-020 towards AQP4 [18]. A report from a cell-based assay could not reproduce the inhibitory results [30]. Another compound with an appropriate affinity for AQP4 is the Aeromics/Simcere drug, AER-270, an investigational drug that was found to reduce cerebral edema. The effect was, however, only a 20% maximal inhibition of human AQP4 [21], which is a little less than the inhibitory effect observed in the present study (approximately 35%). It is reasonable to suspect that the experimental approach or different species holds the explanation. AER-271 has successfully completed a Phase I study but is not yet approved by any regulatory agency. Of note, AER-270 is also a known nuclear factor (NF) κ B pathway inhibitor (usually under the name IMD-0354; IKK2 Inhibitor V; or N-(3,5bis(trifluoromethyl)phenyl)-5-chloro-2-hydroxybenzamide) [21]. The prodrug of AER-270, AER-271, selectively and effectively reduced AQP4-mediated cerebral edema and improved the neurological outcome in a rodent model of transient MCAO [17] but was ineffective in reducing cerebral edema in various traumatic brain injury models [35,36]. This compound was still subjected to a Phase I trial (NCT03804476, no data reported yet), and a Phase II trial is planned (cerebral edema prevention in acute ischemic stroke). No updates have been released yet.

From these contrasting findings, the search continues for a specific and potentially clinically relevant inhibitor of AQP4 with the same inhibitory effect no matter the test system. We reanalyzed the structure of TGN-020 [20] and identified a novel tautomer. As evident from the COSMO-RS sigma-surface, the ORI-TRN-002 compound provides the new hydrogen-bonding pattern and supports the novel tautomer as the viable target structure for AQP4. This finding contrasts the commonly used structure as reported by the X-ray analysis in [20]. Our new structure for TGN-020 is, however, not without precedence. The exo-imine tautomer of the aminothiadiaazole moiety is present in the X-ray structure of 2-Cyano-3-{4-[2-(2,6-dimethyl-phenoxy)-ethoxy]-3-methoxy-phenyl}-N-(5-tert-butyl- [1,3,4]thiadiazol-2-yl)-acrylamide, which adds plausibility to our findings. ORI-TRN-002 supersedes solubility and free fraction limitations of another reported AQP4 inhibitor, the Aeromics/Simcere drug [21], which is a feature that requires the compound to be in the form of a phosphate ester prodrug due to solubility limitations. Methodological differences in executing these assays mean that attempts to replicate prior works may also result in equivocal outcomes. Here, we measured the osmotic water permeation through AQP4 expressed in *Xenopus laevis* oocytes using our sensitive volume measurement setup [18]. To ascertain the osmotic water permeability of an AQP4-expressing oocyte, it is imperative to induce the osmotic gradient at a rate surpassing the cell volume change rate. Additionally, data acquisition should be rapid enough to capture multiple points during the initial linear phase of cell volume change. These fundamental technical prerequisites are at times overlooked in the study of AQP-mediated water permeability, and their absence may introduce confounding factors. We found that ORI-TRN-002 blocked AQP4 as efficiently as TGN-020 and AER-270, and the observed inhibition was evident both with pretreatment and upon the acute application of ORI-TRN-002 with an IC_{50} of $\sim 3 \mu\text{M}$. The binding affinity of ORI-TRN-002 is comparable to TGN-020. The binding affinity ultimately depends on the sum of positive and negative energetic contributions to the binding Free Energy, such as hydrogen bonding, electrostatics, van der Waals attractive, desolvation, and conformational energies. The reduction in conformational degrees of freedom can contribute to an improved binding energy. Therefore, the removal of flexibility is indeed a design principle. Usually, however, only freezing freely rotatable sp^3 – sp^3 bonds are taken into account, with 0.3 kcal/mol per such a bond. The hydroxy group in ORI-TRN-002 occupies a space that is not occupied in TGN-020, and could therefore introduce some repulsion or change in desolvation. In conclusion, here, we present ORI-TRN-002 as a novel and efficient inhibitor of AQP4-mediated osmotic water permeability, and with a more energetically stable form than the parent drug compound TGN-020. Docking experiments have so far proved unable to

provide new and more potent AQP4 inhibitors. However, on future ideas to search for even more potent compounds, our new ligand along with the new hydrogen-bonding pattern could undergo an inhibitor optimization process with the calculation of binding models. AQP4 inhibition by ORI-TRN-002 is a novel approach to further address the role of AQP4 in brain water entry and exit as a complementary tool to the AQP4 knock-out strategy [37], and could potentially be used for the pharmacological treatment of pathologies involving excess AQP4-mediated fluid movements.

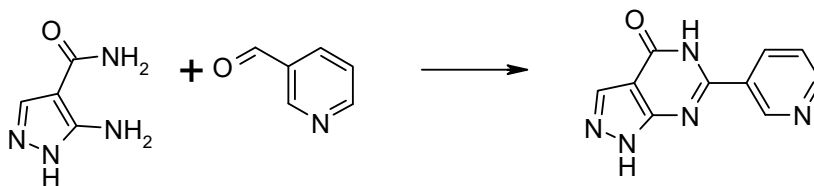
4. Materials and Methods

Tautomer and conformer generation—All compound structures are stored in SMILES format in an in-house database. The chemical structures were desalted and neutralized, if possible. Tautomers were generated for each compound based on the cleaned canonical SMILES strings using an in-house program. For each tautomer, up to ten main conformers were generated using SMILES for 3D conversion and conformational sampling.

COSMO file generation—COSMO files were generated using the TURBOMOLE program (Dassault Systèmes SE, Vélizy-Villacoublay, France) [38,39] and employing geometry optimization with BP-TZVP-COSMO density functional calculation in combination with the COSMO solvation model implemented in TURBOMOLE.

COSMOsim3D calculations—COSMOsim3D was used as described [15] to calculate the σ -surface-based similarity of the tentative bioisosteric pairs, whereby the novel tautomer of TGN-020 was compared with the lowest energy conformer/tautomer of each probe compound. The s-surfaces were extracted from the corresponding cosmo files.

Synthesis and NMR characterization of ORI-TRN-002—(6-(pyridin-3-yl)-1H-pyrazolo[3,4-d]pyrimidin-4(5H)-one) was synthesized and characterized.



5-Amino-1H-pyrazole-4-carboxylic acid amide (5 mmol, 631 mg) and nicotinaldehyde (5 mmol, 536 mg) were dissolved in HOAc (15 mL). DDQ (3.75 mmol, 851 mg) was added, and the mixture was stirred at 140 °C under microwave irradiation. The mixture was filtered, and the filtrate was diluted with EtOAc (75 mL) and filtered again. The combined solids were purified by reversed-phase gradient flash chromatography. Yield 0.45 mmol, 97 mg; HPLC-MS; 98% pure, MH^+ 214.0; 1H NMR (400 MHz, DMSO- d_6) δ = 9.52 (d, J = 2.1 Hz, 1H), 9.14 (ddd, J = 8.3, 2.1, 1.8 Hz, 1H), 9.06 (dd, J = 5.7, 1.8 Hz, 1H), 8.26 (s, 1H), 8.18 (dd, J = 8.3, 5.7 Hz, 1H). The compound is available upon request to M.T., Origenis™.

RNA preparation and heterologous expression in *Xenopus laevis* oocytes—The most prominent isoform of AQP4 in the brain, called M23 due to its translation initiation site at methionine at position 23 in the primary structure of AQP4 [3], was employed for these experiments. cDNA-encoding rat AQP4 was subcloned into an oocyte expression vector, pXOOM, linearized downstream from the poly-A segment and in vitro transcribed using a T7 mMessage machine according to manufacturer's instructions (Ambion, Austin, TX, USA). cRNA was extracted with MEGAClear (Ambion, Austin, TX, USA) and micro-injected into defolliculated *Xenopus laevis* oocytes (EcoCyte Bioscience, Dortmund, Germany); 10 ng RNA was injected per oocyte, and the oocytes were kept in Kulori medium ((in mM) 90 NaCl, 1 KCl, 1 CaCl₂, 1 MgCl₂, 5 HEPES (pH 7.4)) for 3–4 days at 19 °C prior to experiments. AQP4 was stably expressed at the plasma membrane at the time of the experiments as evidenced by immunostaining and functional expression [18].

Volume recordings of oocytes—Oocytes were placed in an experimental recording chamber and perfused with various solutions, and volume measurements were performed, as previously described [40]. Briefly, the oocytes were placed in a small chamber with a

glass bottom and perfused with solutions of interest. The volume of the oocytes was viewed from below via a long-distance objective, and micrographs were captured continuously with a high-resolution recording system (with a high signal-to-noise ratio) based on a CCD camera at a rate of 25 images/s [41]. The control perfusion solution consisted of (in mM) 50 NaCl, 2 KCl, 1 MgCl₂, 1 CaCl₂, 10 HEPES, and 100 mM mannitol (Tris-buffered pH 7.4, 220 mOsm). Hypotonic solutions were subsequently made by the removal of mannitol (Δ100 mM mannitol) with a resulting osmolarity of 120 mOsm. The osmotic water permeability was determined by $L_p = (J_v)/(A \times \Delta\pi \times V_w)$, where J_v is the initial water flux during an osmotic challenge, A is the membrane surface area (nine times the apparent area due to membrane folding [42]), $\Delta\pi$ is the osmotic challenge, and V_w is the partial molal volume of water (18 cm³/mol). Osmolarities of all solutions were verified with an accuracy of 1 mOsm with a Type 15 osmometer (Löser Messtechnik, Berlin, Germany). The compounds used were dissolved in DMSO (controls exposed to vehicle (DMSO) only), and their effect on volume changes were recorded after 10 min of treatment, with the oocytes serving as their own controls or after long-term application, when the oocytes were incubated at 19 °C for 60 min. The determination of compound-mediated effects was carried out in a researcher-blinded fashion.

Data presentation and statistics—All data are given as mean ± SEM. Statistical tests were performed by use of GraphPad Prism 8.4.3 (GraphPad Software Inc., La Jolla, CA, USA). Statistical significance was tested with Student's *t*-test or one-way ANOVA, as stated in the figure legends. *p* values < 0.05 were considered statistically significant. The number of experiments (*n*) corresponds to the independent measurements from two–three different oocyte preparations. The equation $y = 100/(1 + 10^{((\log IC_{50} - x) \times \text{Hill slope}))}$ was used to fit the IC₅₀ curves for each individual experiment, which are shown as summarized.

Author Contributions: Conception and design of research: N.M., M.T. and T.L.T.-B.; analysis of data: G.G., N.T., N.Y., R.K., M.T. and T.L.T.-B.; interpretation of results: N.M., G.G., N.T., N.Y., R.K., M.T. and T.L.T.-B.; preparation of figures: M.T. and T.L.T.-B.; drafting of manuscript: M.T. and T.L.T.-B. All authors have read and agreed to the published version of the manuscript.

Funding: The project was funded by the Lundbeck Foundation (R303-2018-3005 to T.L.T.-B.) and the Weimann Foundation (to T.L.T.-B.).

Data Availability Statement: We confirm that all relevant data from this study are available from the first author upon request.

Conflicts of Interest: M.T. is a co-founder and the CEO/CSO of Origenis GmbH. The authors declare no conflicts of interest. The funders had no role in the design of the study; in the collection, analysis, or interpretation of data; in the writing of the manuscript; or in the decision to publish the results.

Abbreviations

AQP: Aquaporin; AQP4: Aquaporin 4; COSMO-RS: conductor-like Screening Model for Realistic Solvents; DFT: density functional theory; TGN-020: 2-(nicotinamide)-1,3,4-thiadiazole.

References

1. Leinonen, V.; Vanninen, R.; Rauramaa, T. Raised intracranial pressure and brain edema. *Handb. Clin. Neurol.* **2018**, *145*, 25–37.
2. MacAulay, N.; Zeuthen, T. Water transport between CNS compartments: Contributions of aquaporins and cotransporters. *Neuroscience* **2010**, *168*, 941–956. [[CrossRef](#)]
3. Amiry-Moghaddam, M.; Ottersen, O.P. The molecular basis of water transport in the brain. *Nat. Rev. Neurosci.* **2003**, *4*, 991–1001. [[CrossRef](#)]
4. Nielsen, S.; Nagelhus, E.A.; Amiry-Moghaddam, M.; Bourque, C.; Agre, P.; Ottersen, O.P. Specialized membrane domains for water transport in glial cells: High-resolution immunogold cytochemistry of aquaporin-4 in rat brain. *J. Neurosci.* **1997**, *17*, 171–180. [[CrossRef](#)] [[PubMed](#)]
5. Nagelhus, E.A.; Ottersen, O.P. Physiological roles of aquaporin-4 in brain. *Physiol. Rev.* **2013**, *93*, 1543–1562. [[CrossRef](#)] [[PubMed](#)]
6. Papadopoulos, M.C.; Verkman, A.S. Aquaporin-4 and brain edema. *Pediatr. Nephrol.* **2007**, *22*, 778–784. [[CrossRef](#)]

7. Manley, G.T.; Fujimura, M.; Ma, T.; Noshita, N.; Filiz, F.; Bollen, A.W.; Chan, P.; Verkman, A.S. Aquaporin-4 deletion in mice reduces brain edema after acute water intoxication and ischemic stroke. *Nat. Med.* **2000**, *6*, 159–163. [[CrossRef](#)]
8. Manley, G.T.; Binder, D.K.; Papadopoulos, M.C.; Verkman, A.S. New insights into water transport and edema in the central nervous system from phenotype analysis of aquaporin-4 null mice. *Neuroscience* **2004**, *129*, 983–991. [[CrossRef](#)]
9. Haj-Yasein, N.N.; Vindedal, G.F.; Eilert-Olsen, M.; Gundersen, G.A.; Skare, Ø.; Laake, P.; Klungland, A.; Thorén, A.E.; Burkhardt, J.M.; Ottersen, O.P.; et al. Glial-conditional deletion of aquaporin-4 (Aqp4) reduces blood-brain water uptake and confers barrier function on perivascular astrocyte endfeet. *Proc. Natl. Acad. Sci. USA* **2011**, *108*, 17815–17820. [[CrossRef](#)]
10. Yao, X.; Hrabetova, S.; Nicholson, C.; Manley, G.T. Aquaporin-4-deficient mice have increased extracellular space without tortuosity change. *J. Neurosci.* **2008**, *28*, 5460–5464. [[CrossRef](#)]
11. Strohschein, S.; Hüttmann, K.; Gabriel, S.; Binder, D.K.; Heinemann, U.; Steinhäuser, C. Impact of aquaporin-4 channels on K⁺ buffering and gap junction coupling in the hippocampus. *Glia* **2011**, *59*, 973–980. [[CrossRef](#)]
12. Zeng, X.-N.; Sun, X.-L.; Gao, L.; Fan, Y.; Ding, J.-H.; Hu, G. Aquaporin-4 deficiency down-regulates glutamate uptake and GLT-1 expression in astrocytes. *Mol. Cell Neurosci.* **2007**, *34*, 34–39. [[CrossRef](#)]
13. Bill, R.M.; Hedfalk, K. Aquaporins—Expression, purification and characterization. *Biochim. Biophys. Acta Biomembr.* **2021**, *1863*, 183650. [[CrossRef](#)] [[PubMed](#)]
14. Huber, V.J.; Tsujita, M.; Nakada, T. Identification of aquaporin 4 inhibitors using in vitro and in silico methods. *Bioorg. Med. Chem.* **2009**, *17*, 411–417. [[CrossRef](#)]
15. Huber, V.J.; Tsujita, M.; Yamazaki, M.; Sakimura, K.; Nakada, T. Identification of arylsulfonamides as Aquaporin 4 inhibitors. *Bioorg. Med. Chem. Lett.* **2007**, *17*, 1270–1273. [[CrossRef](#)]
16. Thormann, M.; Klamt, A.; Wichmann, K. COSMOsim3D: 3D-similarity and alignment based on COSMO polarization charge densities. *J. Chem. Inf. Model* **2012**, *52*, 2149–2156. [[CrossRef](#)] [[PubMed](#)]
17. Detmers, F.J.; de Groot, B.L.; Müller, E.M.; Hinton, A.; Konings, I.B.; Sze, M.; Flitsch, S.L.; Grubmüller, H.; Deen, P.M. Quaternary ammonium compounds as water channel blockers. Specificity, potency, and site of action. *J. Biol. Chem.* **2006**, *281*, 14207–14214. [[CrossRef](#)]
18. Toft-Bertelsen, T.L.; Larsen, B.R.; Christensen, S.K.; Khandelia, H.; Waagepetersen, H.S.; MacAulay, N. Clearance of activity-evoked K⁺ transients and associated glia cell swelling occur independently of AQP4: A study with an isoform-selective AQP4 inhibitor. *Glia* **2021**, *69*, 28–41. [[CrossRef](#)]
19. Klamt, A.; Thormann, M.; Wichmann, K.; Tosco, P. COSMOsar3D: Molecular field analysis based on local COSMO sigma-profiles. *J. Chem. Inf. Model* **2012**, *52*, 2157–2164. [[CrossRef](#)]
20. Burnett, M.E.; Johnston, H.M.; Green, K.N. Structural characterization of the aquaporin inhibitor 2-nicotinamido-1,3,4-thiadiazole. *Acta Crystallogr. C Struct. Chem.* **2015**, *71*, 1074–1079. [[CrossRef](#)]
21. Farr, G.W.; Hall, C.H.; Farr, S.M.; Wade, R.; Detzel, J.M.; Adams, A.G.; Buch, J.M.; Beahm, D.L.; Flask, C.A.; Xu, K.; et al. Functionalized Phenylbenzamides Inhibit Aquaporin-4 Reducing Cerebral Edema and Improving Outcome in Two Models of CNS Injury. *Neuroscience* **2019**, *404*, 484–498. [[CrossRef](#)]
22. Meinild, A.K.; Klaerke, D.A.; Zeuthen, T. Bidirectional water fluxes and specificity for small hydrophilic molecules in aquaporins 0–5. *J. Biol. Chem.* **1998**, *273*, 32446–32451. [[CrossRef](#)] [[PubMed](#)]
23. Papadopoulos, M.C.; Verkman, A.S. Aquaporin water channels in the nervous system. *Nat. Rev. Neurosci.* **2013**, *14*, 265–277. [[CrossRef](#)] [[PubMed](#)]
24. Tang, G.H.; Yang, G.Y. Aquaporin-4: A Potential Therapeutic Target for Cerebral Edema. *Int. J. Mol. Sci.* **2016**, *17*, 1413. [[CrossRef](#)] [[PubMed](#)]
25. Igarashi, H.; Huber, V.J.; Tsujita, M.; Nakada, T. Pretreatment with a novel aquaporin 4 inhibitor, TGN-020, significantly reduces ischemic cerebral edema. *Neurol. Sci.* **2011**, *32*, 113–116. [[CrossRef](#)]
26. Nakano, T.; Nishigami, C.; Irie, K.; Shigemori, Y.; Sano, K.; Yamashita, Y.; Myose, T.; Tominaga, K.; Matsuo, K.; Nakamura, Y.; et al. Prevents Brain Edema after Cerebral Ischemic Stroke by Inhibiting Aquaporin 4 Upregulation in Mice. *J. Stroke Cerebrovasc.* **2018**, *27*, 758–763. [[CrossRef](#)] [[PubMed](#)]
27. Tradtrantip, L.; Jin, B.J.; Yao, X.M.; Anderson, M.O.; Verkman, A.S. Aquaporin-Targeted Therapeutics: State-of-the-Field. *Adv. Exp. Med. Biol.* **2017**, *969*, 239–250. [[PubMed](#)]
28. Huber, V.J.; Tsujita, M.; Kwee, I.L.; Nakada, T. Inhibition of aquaporin 4 by antiepileptic drugs. *Bioorg. Med. Chem.* **2009**, *17*, 418–424. [[CrossRef](#)]
29. Migliati, E.; Meurice, N.; DuBois, P.; Fang, J.S.; Somasekharan, S.; Beckett, E.; Flynn, G.; Yool, A.J. Inhibition of aquaporin-1 and aquaporin-4 water permeability by a derivative of the loop diuretic bumetanide acting at an internal pore-occluding binding site. *Mol. Pharmacol.* **2009**, *76*, 105–112. [[CrossRef](#)]
30. Verkman, A.S.; Smith, A.J.; Phuan, P.W.; Tradtrantip, L.; Anderson, M.O. The aquaporin-4 water channel as a potential drug target in neurological disorders. *Expert. Opin. Ther. Tar.* **2017**, *21*, 1161–1170. [[CrossRef](#)]
31. Abir-Awan, M.; Kitchen, P.; Salman, M.M.; Conner, M.T.; Conner, A.C.; Bill, R.M. Inhibitors of Mammalian Aquaporin Water Channels. *Int. J. Mol. Sci.* **2019**, *20*, 1589. [[CrossRef](#)]
32. Mola, M.G.; Nicchia, G.P.; Svelto, M.; Spray, D.C.; Frigeri, A. Automated cell-based assay for screening of aquaporin inhibitors. *Anal. Chem.* **2009**, *81*, 8219–8229. [[CrossRef](#)] [[PubMed](#)]

33. Huber, V.J.; Tsujita, M.; Nakada, T. Aquaporins in drug discovery and pharmacotherapy. *Mol. Asp. Med.* **2012**, *33*, 691–703. [[CrossRef](#)] [[PubMed](#)]
34. Wang, F.; Feng, X.C.; Li, Y.M.; Yang, H.; Ma, T.H. Aquaporins as potential drug targets. *Acta Pharmacol. Sin.* **2006**, *27*, 395–401. [[CrossRef](#)] [[PubMed](#)]
35. Wallisch, J.; Jha, R.; Vagni, V.; Feldman, K.; Dixon, C.; Farr, G.; Kochanek, P. Effect of the Novel Aquaporin-4 Antagonist Aer-271 in Combined Tbi Plus Hemorrhagic Shock in Mice. *Crit. Care Med.* **2015**, *43*, 6–7. [[CrossRef](#)]
36. Kochanek, P.M.; Bramlett, H.M.; Dixon, C.E.; Dietrich, W.D.; Mondello, S.; Wang, K.K.W.; Hayes, R.L.; Lafrenaye, A.; Povlishock, J.T.; Tortella, F.C.; et al. Operation Brain Trauma Therapy: 2016 Update. *Mil. Med.* **2018**, *183*, 303–312. [[CrossRef](#)]
37. Eilert-Olsen, M.; Haj-Yasein, N.N.; Vindedal, G.F.; Enger, R.; Gundersen, G.A.; Hoddevik, E.H.; Petersen, P.H.; Haug, F.-M.S.; Skare, Ø.; Adams, M.E.; et al. Deletion of aquaporin-4 changes the perivascular glial protein scaffold without disrupting the brain endothelial barrier. *Glia* **2012**, *60*, 432–440. [[CrossRef](#)] [[PubMed](#)]
38. Balasubramani, S.G.; Chen, G.P.; Coriani, S.; Diedenhofen, M.; Frank, M.S.; Franzke, Y.J.; Furche, F.; Grotjahn, R.; Harding, M.E.; Hättig, C.; et al. TURBOMOLE: Modular program suite for quantum-chemical and condensed-matter simulations. *J. Chem. Phys.* **2020**, *152*, 184107. [[CrossRef](#)]
39. Schäfer, A.; Klant, A.; Sattel, D.; Lohrenz, J.C.W.; Eckert, F. COSMO Implementation in TURBOMOLE:: Extension of an efficient quantum chemical code towards liquid systems. *Phys. Chem. Chem. Phys.* **2000**, *2*, 2187–2193. [[CrossRef](#)]
40. Zeuthen, T.; Zeuthen, E.; Macaulay, N. Water transport by GLUT2 expressed in *Xenopus laevis* oocytes. *J. Physiol.* **2007**, *579*, 345–361. [[CrossRef](#)]
41. Zeuthen, T.; Belhage, B.; Zeuthen, E. Water transport by Na⁺-coupled cotransporters of glucose (SGLT1) and of iodide (NIS). The dependence of substrate size studied at high resolution. *J. Physiol.* **2006**, *570*, 485–499. [[CrossRef](#)] [[PubMed](#)]
42. Zampighi, G.A.; Kreman, M.; Boorer, K.J.; Loo, D.D.F.; Bezanilla, F.; Chandy, G.; Hall, J.E.; Wright, E.M. A method for determining the unitary functional capacity of cloned channels and transporters expressed in *Xenopus laevis* oocytes. *J. Membr. Biol.* **1995**, *148*, 65–78. [[CrossRef](#)] [[PubMed](#)]

Disclaimer/Publisher’s Note: The statements, opinions and data contained in all publications are solely those of the individual author(s) and contributor(s) and not of MDPI and/or the editor(s). MDPI and/or the editor(s) disclaim responsibility for any injury to people or property resulting from any ideas, methods, instructions or products referred to in the content.